# Looping Star fMRI in Cognitive Tasks and Resting State

Beatriz Dionisio-Parra, MSc,[1,2*] Florian Wiesinger, PhD,[2] Philipp G. Sämann, MD,[3] Michael Czisch, PhD,[3†] and Ana Beatriz Solana, PhD[2†]

**Background:** Conventional $T_2$*-weighted functional magnetic resonance imaging (fMRI) is performed with echo-planar imaging (EPI) sequences that create substantial acoustic noise. The loud acoustic noise not only affects the activation of the auditory cortex, but may also interfere with resting state and task fMRI experiments.
**Purpose:** To demonstrate the feasibility of a novel, quiet, $T_2$*, whole-brain blood oxygenation level-dependent (BOLD)-fMRI method, termed Looping Star, compared to conventional multislice gradient-echo EPI.
**Study Type:** Prospective.
**Phantom/Subjects:** Glover stability QA phantom; 10 healthy volunteers.
**Field Strength/Sequence:** 3.0T: gradient echo (GE)-EPI and $T_2$* Looping Star fMRI.
**Assessment:** Looping Star fMRI was presented and compared to GE-EPI with a working memory (WM) task and resting state (RS) experiments. Temporal stability and acoustic measurements were obtained for both methods. Functional maps and activation accuracy were compared to evaluate the performance of the novel sequence.
**Statistical Tests:** Mean and standard deviation values were analyzed for temporal stability and acoustic noise tests. Activation maps were assessed with one-sample *t*-tests and contrast estimates (CE). Paired *t*-tests and receiver operator characteristic (ROC) were used to compare fMRI sensitivity and performance.
**Results:** Looping Star presented a 98% reduction in sound pressure compared with GE-EPI, with stable temporal stability (0.09% percent fluctuation), but reduced temporal signal-to-noise ratio (tSNR) (mean difference = 15.9%). The novel method yielded consistent activations for RS and WM (83.4% and 69.5% relative BOLD sensitivity), which increased with task difficulty (mean CE 2-back = 0.56 vs. 0-back = 0.08, $P < 0.05$). A few differences in spatial activations were found between sequences, leading to a 4–8% lower activation accuracy with Looping Star.
**Data Conclusion:** Looping Star provides a suitable approach for whole-brain coverage with sufficient spatiotemporal resolution and BOLD sensitivity, with only 0.5 dB above ambient noise. From the comparison with GE-EPI, further developments of Looping Star fMRI should target increased sensitivity and spatial specificity for both RS and task experiments.
**Level of Evidence:** 2.
**Technical Efficacy Stage:** 1

J. MAGN. RESON. IMAGING 2020.

## Introduction

Although functional magnetic resonance imaging (fMRI) has evolved into the dominant tool for noninvasively imaging human brain activity, the loud acoustic noise inside the scanner during acquisition remains a major concern, as it causes discomfort and anxiety in patients[1] and may interfere with the brain response under investigation.[2–4]

Gradient-echo echo-planar imaging (GE-EPI) is the most commonly used pulse sequence for fMRI because of its rapid image acquisition and excellent sensitivity to the blood oxygen level-dependent (BOLD) effect.[5] However, this pulse

View this article online at wileyonlinelibrary.com. DOI: 10.1002/jmri.27073

Received Jul 31, 2019, Accepted for publication Jan 13, 2020.

*Address reprint requests to: B.D.P., TUM Graduate School of Bioengineering, Technical University of Munich, Boltzmannstr. 11, D-85748 Garching, Germany. E-mail: beatriz.dionisio@tum.de
†Both authors contributed equally to this manuscript.

Contract grant sponsor: With the support of BERTI, a multipartner Initial Training Network under the European Union program FP7-PEOPLE-2013-ITN.

From the [1]Department of Computer Science, Technical University of Munich, Garching, Germany; [2]ASL Europe, GE Healthcare, Munich, Germany; and [3]Max Planck Institute of Psychiatry, Munich, Germany

Additional supporting information may be found in the online version of this article

sequence is one of the loudest due to the rapid gradient switching required for the EPI readout.[6]

The loud acoustic noise generated in the MR scanner arises from interactions between the gradient coils and the magnet. During the process of image encoding, the switching of the gradient coils induces Lorentz forces and eddy currents that act on the coils and connecting elements.[7] The induced mechanical vibrations propagate through the surrounding air, generating a progressive sound wave. The noise intensity depends on many factors, including the gradient strength and slew rate, and easily exceeds 100 dB for a 3T scanner,[6,8] being close or even above the human auditory pain level (120–130 dB). Although appropriate earplugs or headphones are commonly used, providing up to 40 dB noise suppression, the remaining noise is still unpleasant and limits the possibility of scanning small children, psychiatric patients, or participants who are particularly bothered by auditory stimulation.

The impact of the scanner acoustic noise is even higher for fMRI experiments, since the acoustic noise interferes with auditory perception and results in a continuous BOLD response,[3,8] which might reduce the ability to detect signals of interest.[4] Although this interference is more problematic when performing auditory or language tasks, it also affects other fMRI experiments, such as motor or visual paradigms, by increasing demands on attention systems.[9–11] In addition, it has been suggested that acoustic noise affects resting state networks (RSNs) in task-free experiments.[12,13]

Several hardware and software attempts have been proposed to reduce acoustic scanner noise.[9] On the hardware side, some approaches have included the use of rotating coils to reduce gradient switching,[3] redesigning the gradient geometry to counterbalance the mechanical vibrations,[7,14] and improving its acoustic isolation.[15] A more sophisticated technique consists of active noise cancellation (ANC),[16] which works through a destructive interference that is sent to the headphones and cancels a portion of the scanner noise. These solutions are far from being practical and the contribution of bone-conducted vibrations lead to residual perceived loudness.

The strategy that is most widely used to avoid the problem of scanner noise in fMRI is sparse imaging, where stimuli are presented during silent periods of the scanning protocol.[4,13] Compared to continuous imaging, this approach requires excessively long scanning times and results in a lack of temporal resolution of the BOLD response. In addition, modifications to EPI sequences were developed to reduce sound levels by changing the gradient pulse shape[17] or using a combination of parameters that varies the speed of gradient switching.[18] This resulted in a reduction of the scanner noise of up to 40 dB, but at the cost of reduced temporal signal-to-noise ratio (tSNR) spatial smoothness and/or signal dropouts.

Zero echo time (Zero TE) pulse sequences were introduced in the 1990s, such as the 3D rotating ultrafast imaging sequence (RUFIS),[19] which experienced a recent revival in the form of SWIFT,[20] ZTE,[21] and PETRA.[22] Zero TE imaging uses short and intense pulse excitation followed by 3D radial sampling to achieve isotropic and large field-of-view (FOV) coverage and nominal TE of zero. With only minimal gradient ramping between repetitions, the pulse sequence is robust against gradient imperfections and behaves as virtually silent. Although Zero TE native contrast is proton density[34], different contrasts can be added through preparation modules before the readout, as in the $T_2$-prepared RUFIS sequence[23] that was developed for quiet fMRI based on $T_2$-weighted contrast. Recently, a novel sequence termed "Looping Star"[24] has been described for $T_2$*-weighted imaging, $T_2$* mapping, quantitative susceptibility mapping (QSM), and $T_2$* BOLD fMRI.

It is the aim of the current work to present and assess the performance of the novel quiet "Looping Star" method[24] for whole-brain $T_2$* BOLD fMRI. Temporal stability and functional sensitivity was assessed for this fMRI approach using working memory (WM) and resting state (RS) experiments, to test the capability of the novel sequence against the standard method GE-EPI.

## Materials and Methods

### *Looping Star Extension to $T_2$* BOLD fMRI*

*ACQUISITION.* Looping Star[24] is a pulse sequence based on the rotating ultra-fast imaging sequence (RUFIS),[19] extended by a gradient-refocusing mechanism to additionally provide $T_2$* contrast, while maintaining its quiet performance. The extension of the Looping Star sequence to be capable of acquiring BOLD-weighted images requires: 1) to obtain a particular echo time (TE) near the $T_2$* of gray matter; 2) a spatial resolution of at least 2–4 mm; and 3) a volume repetition time (TR) on the order of at most 2–4 seconds for determining the sequential order of activation onsets across brain regions.[25]

A schematic pulse sequence diagram for Looping Star fMRI and the corresponding spatial *k*-space trajectory is shown in Fig. 1. First, 3D radial spokes are excited using short RF block pulses and subsequently refocused in the form of gradient echo (GRE). Accordingly, Looping Star captures an initial free-induction-decay (FID) image at TE = 0, followed by GRE images at equidistant TEs. Here, we used a "one-echo" Looping Star protocol, obtaining the gradient echo image at TE = 26.8 msec, which was expected to give sufficient BOLD contrast at 3T. 3D *k*-space is encoded using a radial trajectory, in which the spokes are acquired within an arbitrary closed-trajectory plane inside the 3D sphere (star or circle with equidistant spokes) repeated twice per segment to get the FID and the echo. The initial star was placed at k = 0; then subsequent segments were rotated in a pseudorandom order. The rotation of the segments (star or circles) was iteratively optimized for sampling uniformity, selecting each consecutive segment (from 20 possible tests) by minimizing the overall electrical potential of an equivalent distribution of charged point sources.[24]

*PARAMETER SELECTION.* In order to match a standard clinical protocol for fMRI, we adjusted Looping Star to achieve a spatial resolution of 3 mm isovoxel, a TE between 25–35 msec, and a TR lower

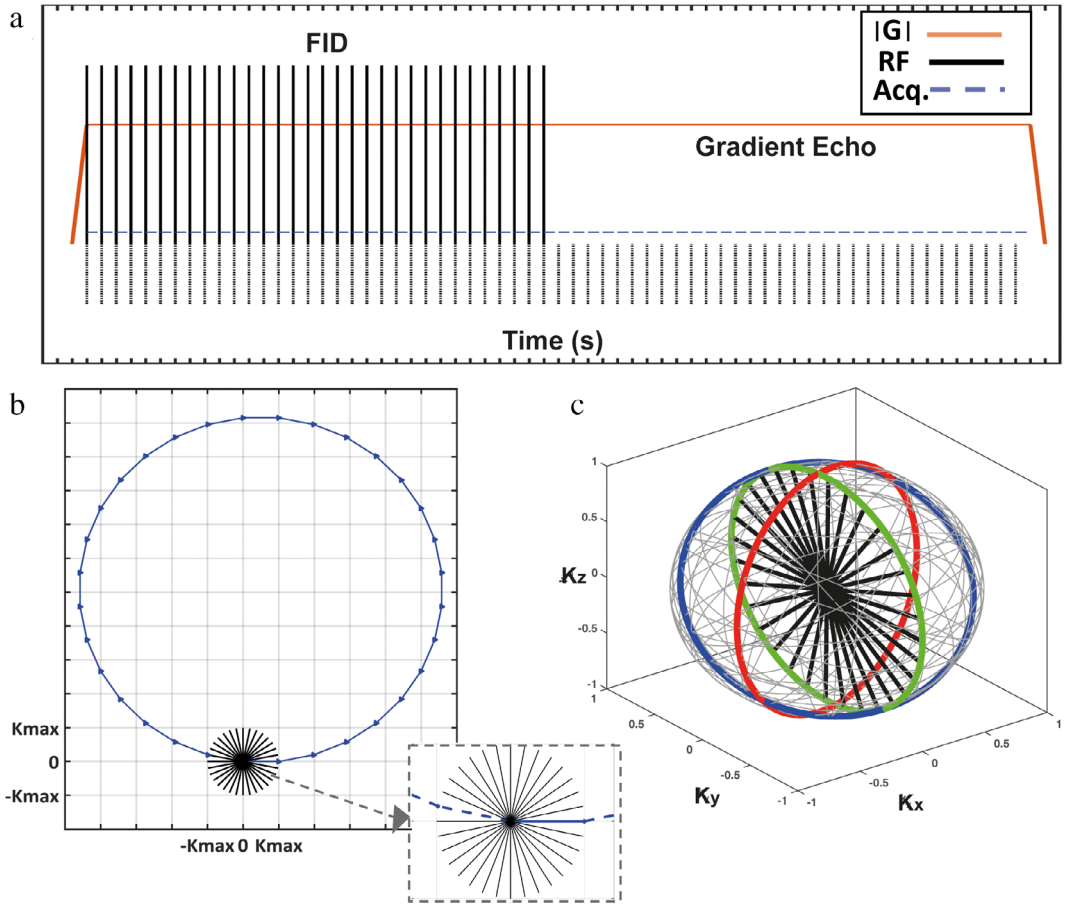


**FIGURE 1: Simplified pulse sequence of the Looping Star fMRI experiment collecting one FID and one gradient echo. (a) Gradient waveforms and RF pulses of the one-echo Looping Star acquisition are shown for a single segment with 32 spokes. The readout gradient has constant magnitude with smoothed directional increments by in-plane rotations between consecutive spokes. (b) Corresponding *k*-space encoding for the 32 spokes of the segment, showing the self-refocusing trajectory of the first excitation. (c) 3D spatial encoding via random rotation of the 32 planes (loops) to achieve full 3D *k*-space coverage (total of 1024 spokes per fMRI volume). In green, red, and blue are presented the first, second, and third loops, respectively. The spokes (in black) are represented as straight, although they are slightly bent due to the 14 smoothing factor.**

than 3 seconds. The time per spoke was 840 μs for a resolution of 3 mm (with field of view [FOV] = 19.2 cm and receiver bandwidth [BW] = ±31.25 kHz). TE = 26.8 msec was obtained by using 32 spokes per loop (TE = time_per_spoke*number_spokes_per_loop = 840 μs*32 = 26.8 msec), resulting in a time per segment (64 spokes + gradient rampup and rampdown) of 70 msec. A TR = 2.24 second was then obtained by acquiring 32 different oriented segments per volume (TR = time_per_segment*number_segments = 70 msec*32 = 2.24 seconds), resulting in 1024 spokes per fMRI volume (Fig. 1c). This provided sufficient 3D spatial encoding for full-brain coverage with an additional acceleration factor of four with respect to the radial sampling Nyquist criteria ($4*r^2 = 4*32^2 = 4096$ spokes) including a π undersampling factor with respect to Cartesian sampling. In Looping Star, as well as in RUFIS,[19] the RF pulse width should be less than the sampling time determined by the receiver bandwidth, as the gradient is on during the RF emission. For a receiver bandwidth of ±31.25 kHz, the maximum pulse width was then less than 16 μs (= 1/±31.25 kHz), and so a maximum flip angle (FA) of 3° was allowed (for a pulse width of 12 μs for an excitation hard pulse). However, we chose here a lower FA = 1° to obtain PD weighting with minimal transient $T_1$ effects (dynamic equilibrium of the longitudinal magnetization) and to minimize higher-order RF refocusing echoes.[24] All RF pulses were in phase. The FA is also relevant to analyze the sensitivity of Looping Star to in-flow effects. Blood in-flow has two opposite effects. On the one hand, fresh unsaturated blood entering the saturated imaging volume can cause hyperintensity; however, by using a low FA = 1° that effect can be considered negligible. On the other hand, the flow encoding effect of the sinusoidal gradient trajectory imposes a strong motion encoding (very low velocity encoding [VENC], representing the velocity causing π phase). The VENC of Looping Star was estimated as VENC >0.3 cm/s,[24] where small fractions of turbulent flow jointly with changes in the flow encoding direction (dependent on the orientation of the loops) results in flow suppression.

*RECONSTRUCTION.* Looping Star image reconstruction was based on 3D nearest-neighbor gridding, followed by Fourier transformation and root-sum-of-square coil combination,[24] performed offline using MatLab R2015B (MathWorks, Natick, MA). The *k*-space trajectory used for image reconstruction was derived from the nominal gradient waveform prescribed in the pulse sequence.

Looping Star refocused echoes contained the information of the echo-out from spoke *i* (from center of *k*-space to the outer part of *k*-space) and the echo-in from spoke *i + 1* (from the outer part of the *k*-space towards the center of *k*-space).[24] We refer to this phenomenon as echo-in/echo-out mixing and we consider the echo-in as the contaminating signal. To separate the echo-in/echo-out contributions, each segment can be acquired twice, with and without a $\pi$ RF-phase cycling between consecutive excitations. Then the echo-in and echo-out contributions can be separated by means of a simple linear combination without loss of resolution. However, this method doubles the scan time per segment, making it impractical for fMRI. In order to minimize the echo-in contamination, another method is applied, which assumes that echo-out signals dominate at the beginning, and echo-in signals at the end, of a single spoke acquisition. Based on this assumption, a Fermi filter (cutoff =70%) was applied to the gradient-echo spokes, which reduces the image resolution (≈4 mm isovoxel, ie, 70% less spatial resolution) but improves the SNR. Figure S1 in the Supplemental Material illustrates the result of the reconstruction without any echo-in/echo-out correction, after RF phase-cycling combination and after Fermi filtering (70%). The images were acquired with a resolution phantom, with the same parameters used in our fMRI study, but without the extra acceleration factor of 4.

Additionally, a phase correction method was performed to correct for dynamic $B_0$ fluctuations, taking as reference the phase at the center of *k*-space.

### Acoustic Noise Measurements

Acoustic noise measurements were performed with a Bruel & Kjaer (Copenhagen, Denmark) integrated sound level meter (Type 2250) and microphone (Type 4189). The system was calibrated using 94 dB and 114 dB noise sources, showing a sensitivity of 52 mV/Pa. Peak (Lpeak [dB]) and A-weighted average (LAeq [dB(A)]) sound pressure levels (SPLs) were measured. The frequency spectrum was analyzed using the FFT Analysis Package (Type BZ-7230), with a frequency span from 1–20 kHz and 6400 FFT lines, leading to a resolution of 3.125 Hz for the employed Hanning window. For all the measurements, the microphone was placed on top of a spherical agar phantom, inside the head coil at the averaged ear position of a subject. Two measurements, each lasting 30 seconds, were taken in-bore for Looping Star and GE-EPI sequences, as well as in the absence of scanning.

### MR Acquisition

All data were acquired on a 3.0T MR scanner (MR750, GE Healthcare, Chicago, IL) using a 12-channel head coil (MR Instruments, Minneapolis, MN). The parameters of the "one-echo" Looping Star fMRI sequence were adjusted as follows: flip angle = 1°; BW = ±31.25 kHz; uniform and isotropic 3D spatial coverage with FOV = 19.2 cm; matrix size $N$ = 64 points (resulting in a nominal resolution of 3 mm). The effective TE of the FID and GRE images was adjusted as TE = 0 and 26.8 msec, respectively. In all, 1024 radial spokes for the FID and 1024 spokes for the gradient echo were acquired per image volume, distributed over 32 segments (each containing 64 spokes per segment with 840 μs per spoke). The total acquisition time per image volume amounted to TR = 2.24 seconds.

For comparison, equivalent parameters were selected for the conventional GE-EPI sequence, with a matrix size of 64 × 64, FOV = 19.2 cm, slice thickness of 3 mm, and no gap, leading to 3 mm isotropic resolution, with TE = 26.8 msec, with flip angle = 90° and BW = ±250 kHz. The number of axial slices encoded was 32 to equate the 32 segments of Looping Star, resulting in the same TR = 2.24 seconds.

A sagittal high-resolution 3D-$T_1$-weighted inversion-recovery fast-spoiled gradient-echo (3D-IR-FSPGR) was acquired as the anatomical reference and for registration to the Montreal Neurological Institute (MNI152) standard anatomical template. The following parameters were used: TR = 6.14 msec; TE = 2.24 msec; inversion time = 450 msec; FA = 12°; matrix = 256 × 256 × 196; BW = ±62.5 kHz; voxel size = 1 × 1 × 1 $mm^3$, and scan time of 7:12 minutes.

### Data Quality and Temporal Stability Assessment

In order to warrant that our preprocessing pipeline can deal with both types of sequences, distortions and signal dropouts of Looping Star (FID and GRE) and GE-EPI images were compared with the $T_1$-weighted image as reference. The protocol was defined as follows: after a fast review of all LS-FID, LS-GRE, and GE-EPI images for an overview of the quality range, the 10 datasets were shuffled and rated by three independent raters. First, each rater assessed the fit of the brain's margin of the functional image with the anatomical reference in a three-plane overlay view using a 5-point Likert scale (1: no distortion, 5: extreme distortions). For this step, raters were asked to focus on areas with preserved signal. Second, the signal dropout was quantified in the number of axial slices, separated for the lower temporal lobe areas and the medial orbitofrontal areas by subtracting the last correctly represented (lowest) slice on the functional image with the lowest respective slice on the anatomical image. Here, higher differences indicate stronger signal dropout. Ratings of the three raters were averaged and compared between sequence types using paired *t*-tests.

Given the importance of tSNR for fMRI, signal stability measurements from the FBIRN quality assurance protocol[26] were performed and compared between the fMRI methods, using a phantom from the Glover stability QA protocol (17 cm diameter spherical phantom with a doped agar gel[28]). Summary values for signal intensity, standard deviation (SD), percentage fluctuation (RMS), drift, and radius of decorrelation (RDC) were estimated from a 21 × 21 voxel region of interest (ROI) in the center of the phantom. tSNR was calculated as the signal mean divided by the standard deviation across all volumes. To evaluate the effect of the selected flip angle on the tSNR, a comparison analysis with variable FA = [1°, 1.5°, 2°, 2.5°, 3°] for Looping Star was performed. Corresponding tSNR values and maps were compared to GE-EPI, also after smoothing (with a Gaussian kernel of 4 $mm^3$) for better equivalence.

In vivo fMRI data acquired during RS runs underwent the same QA analysis after motion correction, normalization procedures, and extraction of each gray matter (GM) using the MNI152 atlas GM mask. The average of signal stability measurements over all corresponding GM voxels was computed for each subject (mean ± standard deviation).

### Subjects

Ten healthy subjects (eight females), aged $30 \pm 5$ years (mean $\pm$ SD), were recruited after being checked for standard MRI exclusion criteria and general neurological history. All subjects provided written informed consent after a full explanation of the protocol and were reimbursed for their participation. The study protocol was in accordance with the last version of the Helsinki Declaration and approved by the local Ethics Committee.

### Functional Experiments

Subjects performed a letter variant of an N-back task. This paradigm was chosen because it is an established WM paradigm[27] that invokes activations across the whole brain. In brief, a pseudorandom sequence of consonants (500 msec duration) was back-projected in the center of the visual field. The subjects were instructed to press a response button whenever they saw a prespecified target letter (0-back, control condition), or when the current letter was the same as the one before (1-back) or two before (2-back). Conditions were run in blocks of 40 seconds (16 stimuli, 25% targets) alternating with periods of rest (fixation, 40 seconds), during which subjects had to fixate a cross. Each condition was repeated two times in pseudorandom order. A delay of 8.5 seconds between blocks was provided for instructions. In total, the N-back paradigm lasted around 7:28 minutes (200 volumes). All subjects were familiarized with the task using a training session outside the scanner. The order of quiet and conventional fMRI runs was counterbalanced to avoid order effects.

In addition, participants underwent a resting state (RS)-fMRI acquisition of 8 minutes (220 volumes) for both sequences, to investigate and compare the capability of Looping Star to detect resting state networks (RSNs). Subjects were instructed to remain still and fixating through the head coil mirror. The RS experiments were always run first during each session to minimize fatigue effects.

### Data Preprocessing

Data processing and analyses were done with Statistical Parametric Maps (SPM12 -www.fil.ion.ucl.ac.uk/spm/software/spm12) and Matlab (MathWorks, Natick, MA). Conventional GE-EPI data was independently corrected for slice acquisition timing difference. This processing step was not required for 3D Looping Star. Motion correction was performed on all fMRI scans using rigid body correction (six parameters). Next, realigned images were coregistered to the 3D-$T_1$W image using an affine transformation (12 parameters). At this point, Looping Star FID was used for the coregistration process to achieve higher spatial accuracy (assuming complete spatial correspondence between echoes). Finally, the 3D-$T_1$W image was normalized to the MNI152 template using an affine transformation and nonlinear deformations. After applying the same spatial deformations to the coregistered Looping Star and GE-EPI data, N-back runs were smoothed with a Gaussian kernel of 8 $mm^3$ full-width at half-maximum and highpass-filtered using a cutoff period of 128 seconds.

The nuisance removal steps were performed differently for the WM and the RS data. For the N-back task, only the six motion parameters derived from the realignment step were included in the first level design matrix as nuisance regressors. For the RS data, nuisance removal was performed with the "CompCor" method,[28] extracting the three first principal components (PCs) from white matter (WM), cerebrospinal fluid (CSF), and whole brain (WB) compartments in MNI space. A nuisance matrix with a total 30 regressors (three PCs from WM, three PCs from CSF, three PCs from WB, six motion parameters; plus all derivatives) was included in a general lineal model (GLM) using the normalized data. After the GLM fitting, the residualized images were smoothed and bandpass-filtered in [0.01–0.1] Hz. Then the resultant RS timecourses were used for the further described seed-based analysis.

### Working Memory Analysis

For the WM experiments, the first-level models (ie, GLM) comprised four task regressors (fixation, 0-back, 1-back, 2-back) via convolution of the block-design paradigm with the canonical hemodynamic response function. The main effects of each task condition (0-back, 1-back, 2-back) were computed to determine the WM load, together with the task-positive contrast (2 > 0-back), using one-sample *t*-tests across subjects and on the second level for each fMRI method. For the purpose of our qualitative analysis, group activations were considered statistically significant for $P < 0.005$ (uncorrected) with a minimum cluster size of 30 voxels. Finally, a paired *t*-test was performed to examine the differential results between Looping Star and GE-EPI for the "2 > 0-back" and its reverse "0 > 2-back". Again, the significance was set to a lenient level of $P < 0.005$ (uncorrected), in order to emphasize possible statistical differences.

### Resting State Analysis

To perform a seed-based correlation analysis of the default mode network (DMN), an ROI of the posterior cingulate cortex (PCC) was selected.[29] For the auditory network, two spherical seeds of 8 mm radius were defined in the left and right primary auditory cortex (coordinates at [55–22 9] and [−41–27 6], respectively). These masks were created in standard space according to the Automated Anatomical Labeling (AAL) atlas.[30] For each participant and fMRI sequence, the mean signal time course was extracted from the RS data within the PCC and auditory seeds (after nuisance removal and filtering, but before spatial smoothing) and included in a first level model as regressor. On the second level, a one-sample *t*-test design was used to compute the results of each fMRI method independently. Again, a paired *t*-test was performed to examine the differential results between Looping Star and GE-EPI for the DMN and auditory network. For both statistical analyses, clusters surviving a threshold of voxelwise $P < 0.001$ (uncorrected) and a threshold on cluster extent of $k > 30$ were deemed significant.

### ROI and Activation Accuracy Analyses

Functional ROIs were defined for both WM and RS analyses to extract the mean contrast estimates (CE) as an indirect marker of sensitivity.[31] The ROIs were determined as the N-back activation clusters reported by a large-scale meta-analysis (*"neurosynth.org"*),[32] divided into seven subclusters (frontolateral [right and left], posterior [right and left], insula [right and left], and cingulate), three for the DMN (medial prefrontal cortex, bilateral inferior temporal, bilateral parietal) and 10 for the auditory network (superior and medial temporal gyrus, precentral cortex, medial frontal gyrus and Heschl's gyrus, all right and left). Paired *t*-tests with the averaged ROIs

**TABLE 1. Mean Acoustic Noise Levels for Looping Star, GE-EPI, and Ambient**

| | LAeq, dB(A) | Lpeak, dB |
|---|---|---|
| GE-EPI | 103.3 ± 0.05 | 114.4 ± 0.11 |
| Looping Star | 71.4 ± 0.04 | 93.6 ± 1.31 |
| Ambient noise | 70.9 ± 0.1 | 89.3 ± 1.21 |

LAeq = A-weighted noise level; Lpeak = peak noise level. Ambient refers to the background noise level in the scanner room.

contrast estimates were used to test for significant differences in sensitivity between fMRI acquisitions.

Finally, receiver operator characteristic (ROC) curves were used for quantitative performance comparison among fMRI methods,[33] taking the respective meta-analysis ("neurosynth.org") activation maps as reference of the "truly active" voxels (for reproducibility). To create the ROC curves, the statistical T-threshold was varied ([−10, 10] for WM and [−30, 30] for RS DMN) to denote the true and false positive fractions (TPF and FPF, respectively) across the second-level statistical maps. The area under the curve (AUC) was calculated as a marker of activation accuracy.

## Results

### *Acoustic Noise Levels*

In-bore acoustic noise measurements during Looping Star fMRI and GE-EPI scanning are shown in Table 1. The Looping Star fMRI sequence achieved up to 31 dB(A) – LAeq and 20 dB – Lpeak acoustic noise reduction compared to the conventional GE-EPI. Since acoustic measurements are based on a logarithmic scale, the difference of 31 dB (A) represents more than a 98% reduction in sound pressure. This corresponded to a noise level increase of only 0.5 dB (A) LAeq and 4.3 dB Lpeak relative to the in-bore ambient noise level.

The acoustic noise spectrum in Fig. 2 shows a strong reduction of the acoustic signal emitted by the quiet sequence, particularly close to the ambient level in the low-frequency range (below 7 kHz). Both sequences presented a repetitive pattern at 14.28 Hz, generated by the acquisition of repeated segments or slices (of 70 msec acquisition time). Those components were generally higher for GE-EPI, as can be seen in the insert of Fig. 2. Looping Star is perceived as a continuous background sound due to the minimal directional changes applied to the readout gradient. However, the gradient update within each spoke (time_per_spoke/14 = 60 μs) generates a prominent noise component at about 16.6 kHz (and its harmonic at 8.3 kHz), which is convolved with components generated by additional gradient changes, ie, ramps between segments with long rise and fall times of 2–8 msec. This together with the rapid RF excitation prevents Looping

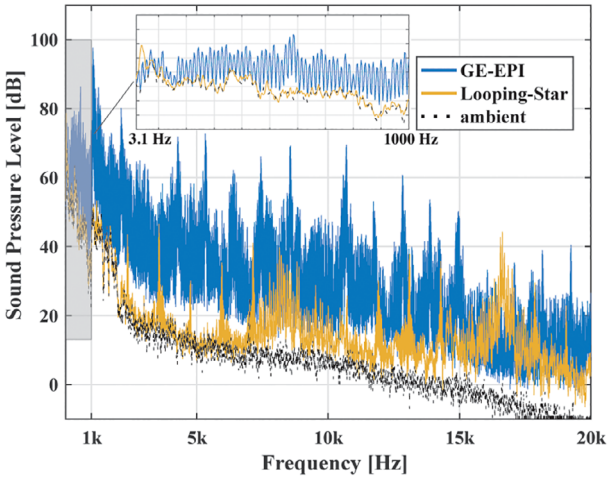


**FIGURE 2: Measured acoustic frequency spectrum of the quiet Looping Star (orange), conventional GE-EPI (blue), and ambient noise (black). Insert shows the low-frequency range from 1 Hz to 1 kHz (with spectral resolution of 3.125 Hz).**

Star from being completely silent. Another higher SPL peak for Looping Star appeared at 40.6 Hz, which might originate from the mechanical response of the MR scanner and remains outside the sensitive part of the human hearing range (ie, 2 kHz – 5 kHz). In contrast, the GE-EPI sequence was characterized by a prominent component located at 1.06 kHz (97.67 dB), with consecutive harmonics of significant intensity, which corresponds to the rapid gradient switching during the readout train.

### *Image Quality and Temporal Stability*

Figure 3a shows one representative volume from a single subject (GE-EPI, Looping Star GRE and Looping Star FID) in comparison with the anatomical reference (3D-$T_1$W). Regarding distortions, no significant differences were detected between the LS-FID and GE-EPI (1.8 ± 0.4 vs. 1.7 ± 0.2, $P$ = 0.224). LS-GRE showed significantly stronger distortions (blurring) (3.0 ± 0.5) compared with both the LS-FID image and GE-EPI ($P = 1.6 \times 10^{-4}$ and $P = 2.0 \times 10^{-5}$). Signal dropouts were present in both GE-EPI and LS-GRE, yet significantly stronger in LS-GRE (33.9 ± 3.3 vs. 15.6 ± 3.0 slices for medial orbitofrontal area, $P$ = 9.4 × 10–9; 18.3 + 2.8 vs. 12.6+/−2.9 slices for lower temporal lobe areas, $P = 6.7 \times 10^{-5}$). Accordingly, as shown in the group tSNR maps (Fig. 3b), Looping Star presented particularly lower tSNR values in the mentioned affected areas, leading to a mean of 15.9% reduction of the tSNR in GM with respect to GE-EPI. Moreover, FBIRN parameters (Table 2) showed comparable temporal stability in both fMRI methods. Percent fluctuations measured in the phantom indicated typical stable values (0.09% for Looping Star and 0.06% for GE-EPI), with a similar small drift (0.56% for Looping Star and 0.69% for GE-EPI). The lower RDC value in Looping Star (6.8 compared to 7.9 in GE-EPI) might represent its spatial

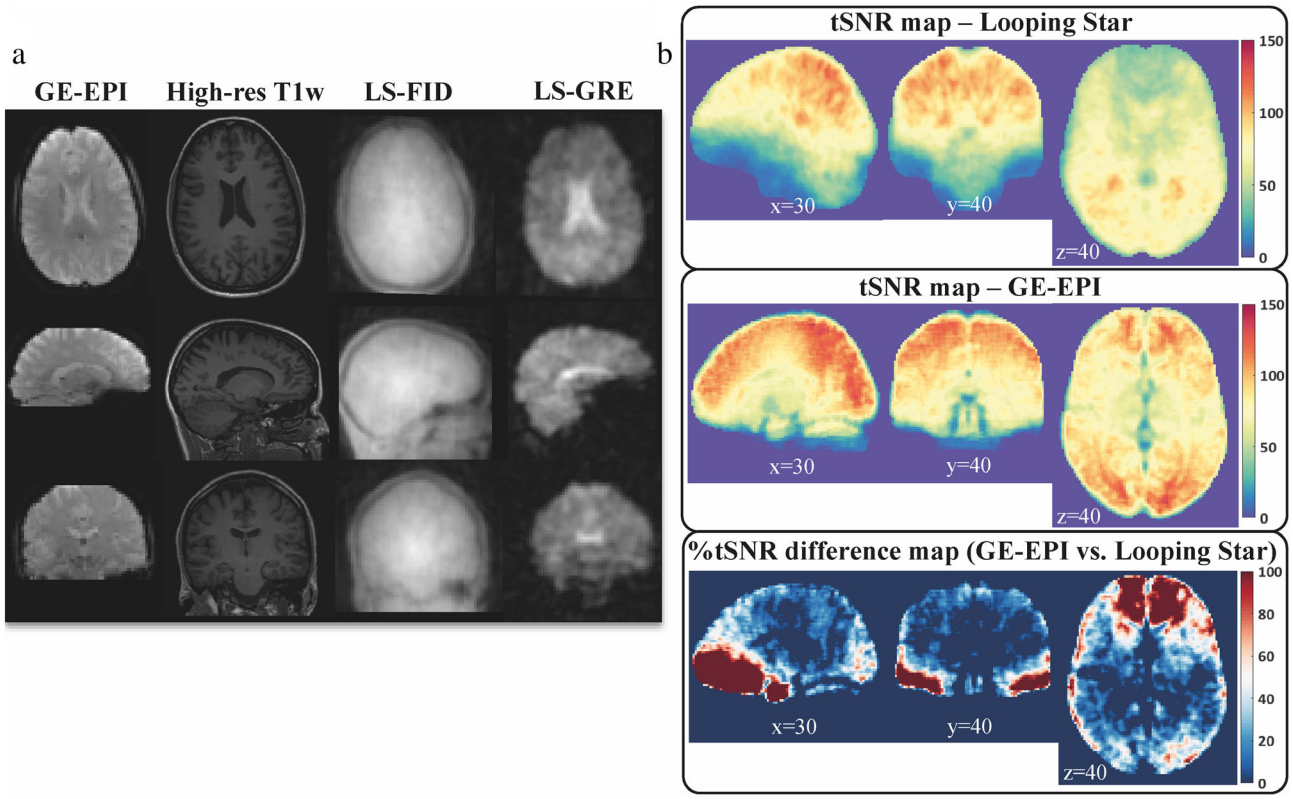


**FIGURE 3: (a) Identical coordinates for axial, sagittal, and coronal views for (left to right) GE-EPI, high-resolution 3D-$T_1$W, Looping Star FID (echo = 0 image), and Looping Star GRE using the prescription for the N-back and RS experiments. (b) Group-averaged tSNR maps for Looping Star and GE-EPI. The last row shows the percent difference map of tSNR between both fMRI methods (color coded between 0% and 100%).**

smoothness derived from the truncated high spatial frequency information used for echo-in and echo-out separation.[24]

The effect of reducing the FA in Looping Star by 0.5° (from FA = 3° to FA = 1°) resulted a progressive tSNR loss of 16.3% ± 6.3% (mean ± SD). The corresponding tSNR maps and values are presented in Fig. S2 in the Supplemental Material.

### *Working Memory Results*

Figure 4 shows the group activation maps of the task positive contrast (2 > 0-back) from (a) Looping Star and (b) GE-EPI data. For both fMRI methods, activation areas were predominant in a bilateral network that comprises the middle (MFG) and superior (SFG) frontal gyrus, the parietal inferior (IPL) and superior (SPL) lobes, and the cingulate cortex (detailed brain regions and peak voxels are provided in Table S1 in the Supplemental Material). As anticipated, Looping Star appeared to yield a general reduced activation (ie, lower T values and less extended), due to the lower tSNR. Accordingly, the mean CEs in the selected WM-ROI amounted to 0.48 ± 0.49 (mean ± SD across subjects) for Looping Star and 0.69 ± 0.38 for GE-EPI, resulting in a

**TABLE 2. Averaged Signal Stability Measurements in Gray Matter (GM) Across the 10 Subjects**

| | Phantom | | In vivo (RS data) | |
|---|---|---|---|---|
| **FBIRN stability** | **Looping Star** | **GE-EPI** | **Looping Star** | **GE-EPI** |
| tSNR | 166.9 | 224.0 | 56.56 ± 8.94 | 67.25 ± 9.24 |
| Drift (%) | 0.6 | 0.5 | 0.17 ± 0.38 | 0.19 ± 0.21 |
| Fluctuation (%) | 0.09 | 0.06 | 0.26 ± 0.07 | 1.67 ± 0.63 |
| RDC | 6.8 | 7.9 | 3.91 ± 0.80 | 6.93 ± 3.11 |

tSNR = temporal signal-to-noise ratio; RDC = radius of decorrelation (RDC, Weisskoff analysis).

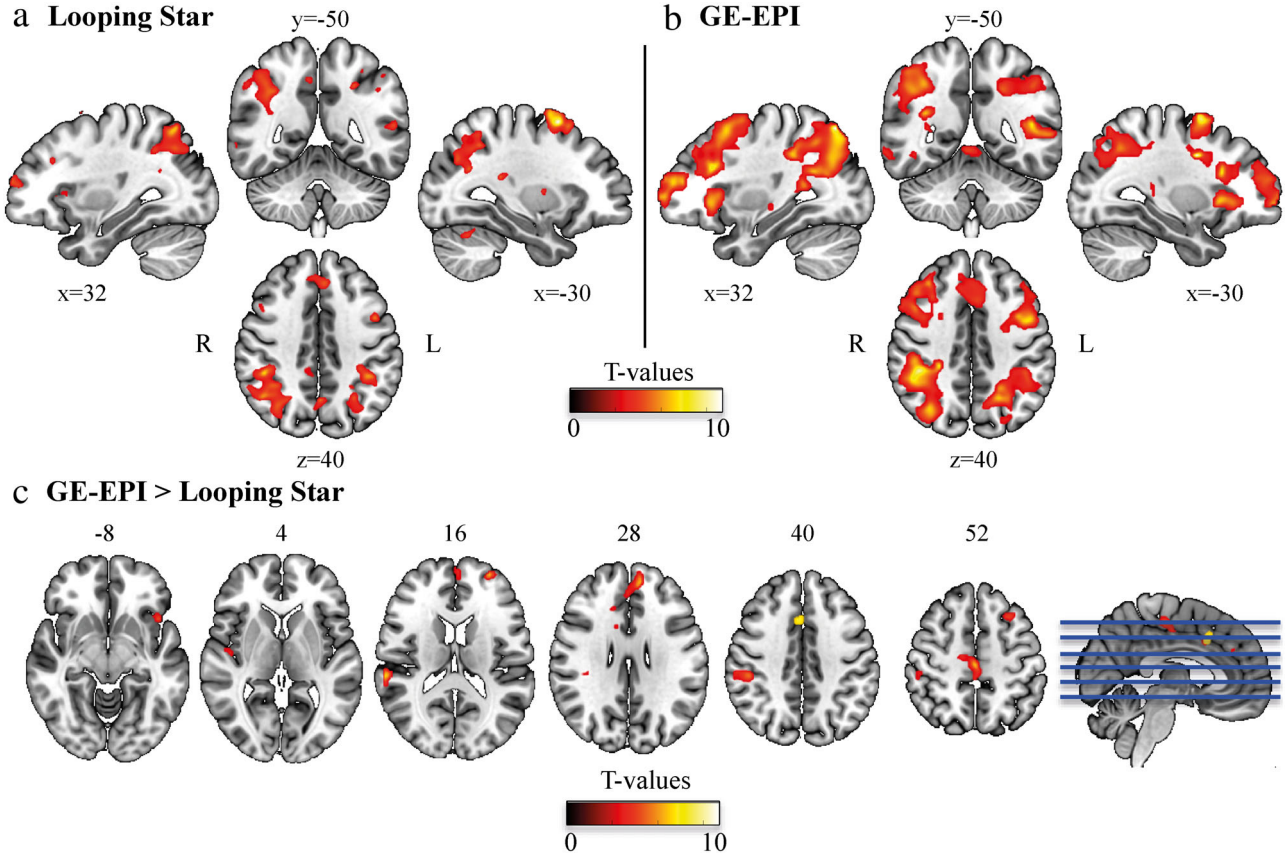


FIGURE 4: Second-level results of the N-back WM task (contrast 2-back>0-back) for (a) Looping Star and (b) GE-EPI. (c) Paired *t*-test GE-EPI > Looping Star of the same contrast. All clusters survived $P < 0.005$ and a cluster extent of $k > 30$. *T*-values are displayed in MNI space for both methods.

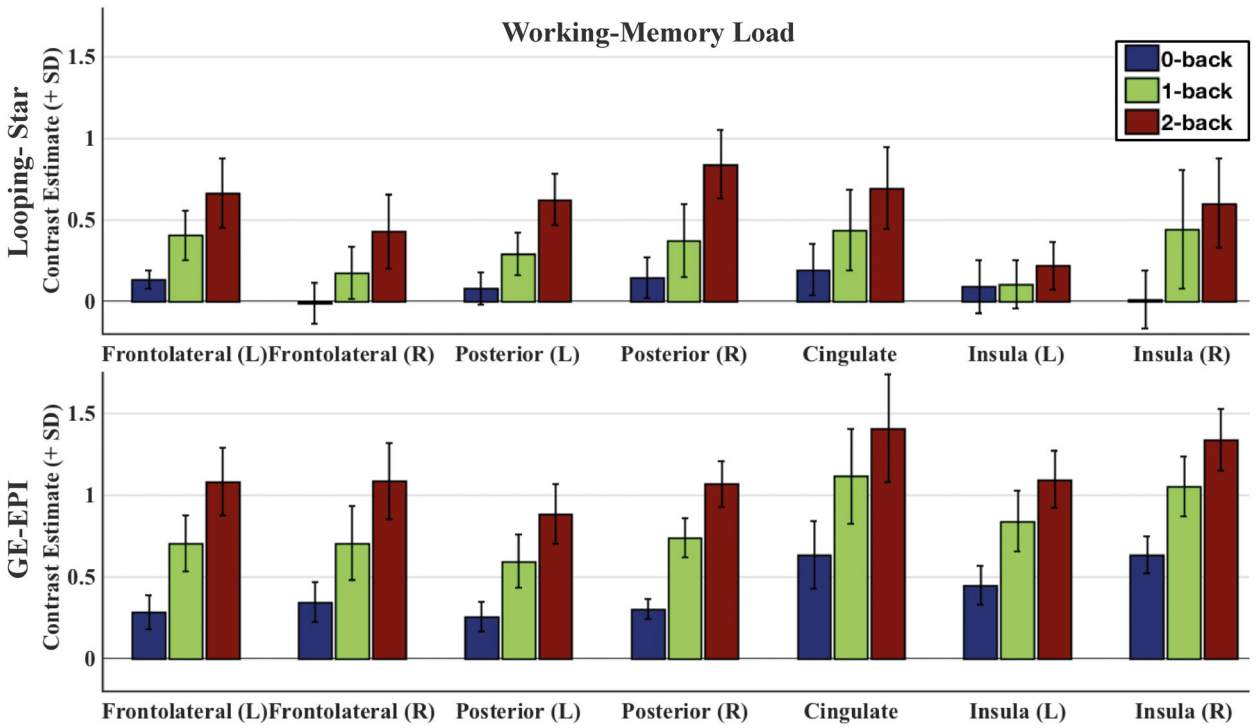


FIGURE 5: WM load during Looping Star and GE-EPI, ie, contrast estimates (mean and SD) of the factor "N-back complexity" (0-back, 1-back, 2-back) across the selected WM subregions.

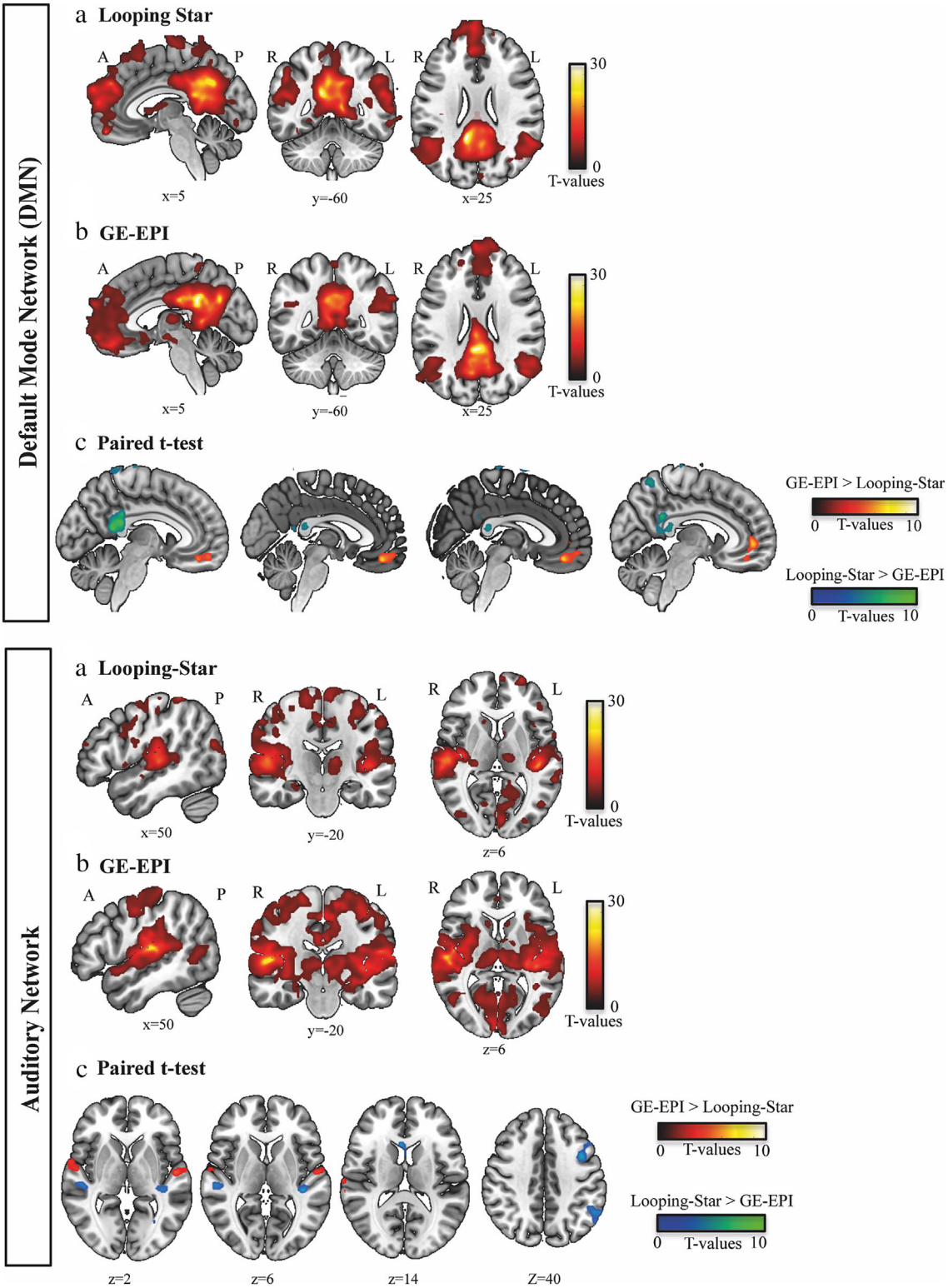


**FIGURE 6: Results of the group DMN (top) and auditory (bottom) seed based analysis (one-sample *t*-tests) on the RS data acquired with (a) Looping Star and (b) GE-EPI. (c) Paired *t*-tests GE-EPI > Looping Star (hot colors) and the reversed Looping Star > GE-EPI (bright colors). All clusters survived a significant threshold of $P < 0.001$ and cluster size of 30 voxels. *T*-values are displayed in MNI space.**

relative BOLD sensitivity of about 69.5% for the quiet sequence with respect to the conventional sequence (see Table S2 in the Supplemental Material for a detailed subregions list of CE results). The larger variation between subjects (ie, average SD) for Looping Star might be attributed to the lower tSNR, further affecting the BOLD sensitivity. The paired *t*-test ($P < 0.005$, uncorrected) shown in Fig. 4c revealed few significant differences for GE-EPI > Looping Star

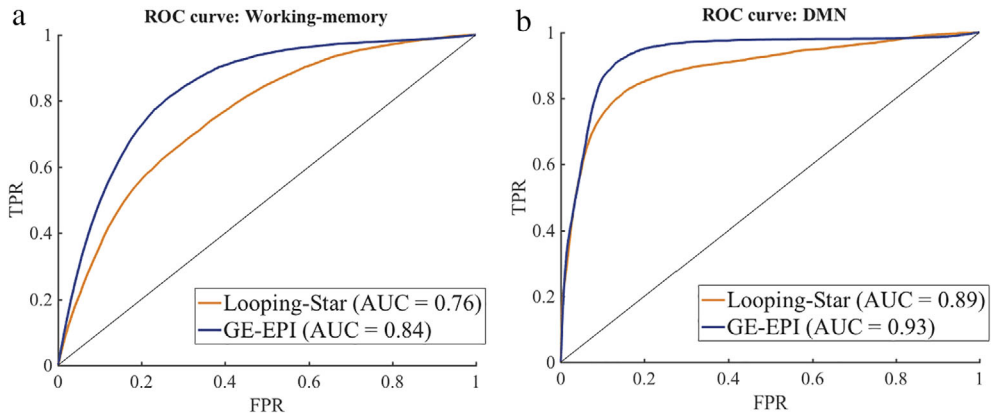


**FIGURE 7: Looping Star and GE-EPI ROC curves of the group activation maps from (a) WM and (b) RS experiments. ROC curves were computed against a reference map (WM network and default-mode-network, respectively) obtained from a large-scale database ("neurosynth.org"). (TPR = true positive rate; FPR = false positive rate; AUC = area under the curve).**

in our sample, with only a cluster in the bilateral cingulate gyrus and middle / superior frontal gyrus within the WM ROI. Additionally, Fig. 5 depicts the measured WM load across subregions of the WM ROI. The quiet sequence successfully showed a consistent increased activation with task difficulty (mean CE 2-back = 0.56 vs. 0-back = 0.08, $P < 0.05$), although presenting lower mean CEs and higher variation than the conventional sequence (particularly in the left insula [$P < 0.05$]).

### *Resting State Results*

The group results of the seed-based RS analysis for the DMN and auditory network are displayed in Fig. 6. In the DMN, both fMRI methods showed similar spatial activation maps, which revealed typical nodes of the DMN, particularly in the adjacent precuneus, the bilateral inferior parietal lobules, and the medial prefrontal cortex (mPFC). The mean CE measured in the total DMN-ROI was only slightly lower for the quiet sequence than for GE-EPI (relative sensitivity of 83.4%) and less variance across subjects than the task-based results (Table S2 in the Supplemental Material). It is worth noting that the comparison of GE-EPI > Looping Star (Fig. 6c, $P < 0.001$ uncorrected) did not yield significant clusters, except for the orbitofrontal region, which can be attributed to the accentuated dropouts for Looping Star. Therefore, the difference in sensitivity (ie, mean CE) was most pronounced ($P < 0.05$) in the medial prefrontal cortex ROI (see also Table S2 in the Supplemental Material for detailed DMN-ROI results). Main activations on the auditory network were found in the bilateral superior temporal gyrus and precentral gyrus, for both fMRI methods. In this case, Looping Star showed less extensive activations than GE-EPI, with also lower CE in the total auditory-ROI (relative sensitivity of 89.6%). However, the mean CEs were higher for Looping Star in the majority of the measured subregions of interest (mean difference = 0.12), except for the superior temporal gyrus (Table S2 in the Supplemental Material). In this region, the paired *t*-test ($P < 0.005$, uncorrected) (Fig. 6, bottom row) showed different clusters for each fMRI method: proximal to the retrosubicular area (Brodmann-48) for GE-EPI > Looping Star, and to Wernicke's area (Brodmann-22) for Looping Star > GE-EPI. This latter contrast also presented a cluster in the prefrontal gyrus.

### *Activation Accuracy With Looping Star fMRI (ROC Results)*

The fitted ROC curves for each experiment are shown in Fig. 7. Looping Star activation accuracy (ie, AUC) was 0.76 for the task experiment and 0.89 for resting state DMN. As expected, Looping Star showed curves relatively closer to the diagonal with smaller AUCs than GE-EPI.

## Discussion

In this study, quiet Looping Star fMRI was tested as an extension of the novel Looping Star sequence[24] and compared with standard GE-EPI using a WM task and RS experiments. The Looping Star fMRI sequence addressed the main limitation of low BOLD sensitivity from the previous $T_2$-prepared ZTE method, while maintaining its favorable characteristics in terms of negligible acoustic noise.

Looping Star demonstrated an overall reduction of the sound levels, particularly close to the ambient noise in the low frequencies (2–5 kHz), in which the human auditory cortex is more susceptible to stimulus presentation.[9] This can be particularly beneficial for presenting stimuli in auditory experiments. In addition, Looping Star changes the nature of the scanner noise in fMRI, producing a continuous sound rather than pulsed, as characteristic in conventional EPI, which may have an impact on human reaction to noise and would need further evaluation.

In terms of image quality, Looping Star provides highly desirable characteristics for fMRI, including: 1) whole brain coverage with good spatiotemporal resolution; 2) sufficient

BOLD sensitivity; and 3) lack of geometrical distortions. Additionally, sampling the central region of *k*-space with each excitation reduces the sensitivity of the technique to motion, assures the same TE for each *k*-space spoke, and allows for the correction of dynamic $B_0$ fluctuations.[35] On the other hand, Looping Star presents moderate levels of off-resonance effects characteristic of the 3D radial acquisitions, due to destructive phase interference at the center of *k*-space where the trajectory repeatedly crosses itself.[36] Thus, the off-resonance effects cause a signal cancellation due to the relative long TE, markedly localized in the orbitofrontal cortex and temporal lobes, which prevent detecting any activation in these regions. Nevertheless, a self-calibrated off-resonance correction method for this 3D radial trajectory could be implemented to alleviate the induced artifacts, eg, by convolution in *k*-space.[36] Alternatively, the multiecho nature of Looping Star offers a practical solution to minimize the susceptibility-related signal loss by echo combination, and to enhance the BOLD sensitivity in the affected areas.[37] Furthermore, Looping Star provides a distortion-free Zero TE FID image, which is advantageous for registration or normalization of the later gradient echoes (ie, the fMRI images in this case), and it would be also useful for R2* fitting in the multiecho approach.

The primary intention of the present investigation was to evaluate the one echo fMRI approach of Looping Star as compared to the conventional GE-EPI, using a block-design paradigm and RS experiments. The WM task is a well-established fMRI paradigm with activations in widespread brain regions. Our results were consistent with a previous WM investigation[10] and revealed increased activations in the frontal and cingulate cortex for the loud sequence (GE-EPI). Moreover, an increased connectivity not only in auditory but also in cognitive RSNs, was reported for RS experiments with low acoustic noise conditions.[12] We found stronger RS-fMRI connectivity in the PCC seed area itself in Looping Star compared with GE-EPI, which may be interpreted as nonlinear differences in sensitivity between the two techniques: possibly hubs with higher functional connectivity are detected more sensitively, whereas medium to low connectivity areas are not affected in the same way. Small differences between both sequences were also found for the auditory network, including the superior temporal gyrus, temporal pole, and prefrontal gyrus. Still, our data demonstrate the feasibility of studying task-related activity as well as resting brain oscillatory networks using the novel Looping Star method. The validation of Looping Star for event-related designs and for acoustic stimulation in particular needs further study.

On the acquisition side, the combination of the desired TE = 26.8 msec and total spokes (1024) to provide sufficient spatial encoding led us to a 3-mm isotropic resolution with a temporal resolution of 2.24 seconds in Looping Star. The GE-EPI acquisition parameters were mainly selected for the optimal comparison with Looping Star, with the same spatial and temporal resolution (3 mm isotropic in 2.24 seconds). The lower FA = 1° was chosen to minimize the contribution of higher-order RF refocusing echoes to the measured signal, although using the Ernst angle (FA = 2.5°) is feasible for the employed Looping Star protocol. The brain coverage was slightly narrower than what can be achieved with multislice GE-EPI sequences (eg, introducing spacing between slices), but it does not deviate from what conventional fMRI studies employ.

For the analysis, special attention was paid to the preprocessing steps in order to avoid introducing any undesired variability due to the different image characteristics. For this reason, the same registration and normalization algorithms were applied to the functional images, with the peculiarity that the FID image was used in the Looping Star registration step due to its larger anatomical information and lack of dropouts. Still, an advantage of the inherent acquisition of the Looping Star FID is the possibility to perform the registration between the mean FID image and the high-resolution $T_1$-weighted scan, with only six parameters to account for residual rigid head movement.

Our functional results showed an effective performance of Looping Star fMRI, detecting activations at the group level for a block-design WM experiment. Although sensitivity was lower compared to conventional GE-EPI, the activation results did not differ significantly and we assume that it might be mainly related to the lower tSNR and dropoff effects. On the other hand, the lower extent of the activations in Looping Star might be related to the in-flow effects and this needs to be investigated.

The activation accuracy analysis with ROC curves revealed that Looping Star is 4–8% less accurate than GE-EPI, for the task and RS experiments, respectively, when both methods are compared with a large-scale meta-analysis activation pattern. Intuitively, the trade-off between false positives and true positives explains the lower activation accuracy of Looping Star at more conservative thresholds, which is associated with its lower sensitivity (ie, absence of active voxels).

Because of the early-stage development of the novel fMRI method, the Looping Star sequence has a wide room for improvement. Further research will be focused on: 1) optimizing both pulse sequence and image reconstruction, to: separate echo-in and echo-out, improve image quality, tSNR, dropoff, and BOLD sensitivity, by incorporating advanced reconstruction techniques like k-t FASTER.[38] Ultimately, as seen in Fig. S2 in the Supplemental Material, a higher FA can be used to maximize the signal, and therefore increase tSNR; 2) investigating the influence of acoustic noise reduction in neural response. Furthermore, Looping Star may be particularly well suited for simultaneous EEG-fMRI studies, since the minimal gradient switching will significantly reduce the gradient-induced artifacts in EEG, and the quiet conditions might enhance detection of evoked potentials.[39]

## Limitations

Several design limitations are present in the current study. First, the experiments were conducted on a reduced sample of 10 healthy subjects and in one MR scanner, limiting the generalizability of our results. Furthermore, the N-back task was repeated twice (plus one session outside the scanner). Although the order of Looping Star and GE-EPI acquisitions was counterbalanced to avoid order effects, it is possible that participants became habituated to the task, reducing the impact of the task difficulty across the presentation of the stimuli. Additionally, a more exhaustive analysis of the RS data, extracting more seed-based networks, or using alternative methods as independent component analysis (ICA), would provide a more extensive assessment of Looping Star compared to conventional sequences.

We also acknowledge that we chose a nonauditory task in order to precisely avoid systematic confounds related to the interference between scanner noise and stimulus presentation and processing.[4] Although it has been reported that acoustic noise also affects cognitive processing,[10,11] we did not contemplate these factors (ie, effect of distraction and/or divided attention by collection of behavioral data) to strictly evaluate the sensitivity of the novel fMRI method as compared to the standard GE-EPI. Moreover, the difference in tSNR between both sequences impedes evaluating this effect alone. Further comparisons with auditory fMRI experiments need to be evaluated for establishing the value of Looping Star, best by including simultaneous event-related potential measurements to further objectify possible differences. In this line, a recent study[40] demonstrated that Looping Star displays good functional sensitivity for acoustic stimulation in spite of reduced signal-to-fluctuation-noise, when compared to EPI using a multiecho acquisition protocol.

## Conclusion

A novel fMRI method with strongly reduced acoustic noise was presented. Our findings demonstrate that the quiet sequence can be used effectively in block-design and RS experiments. In comparison with GE-EPI, Looping Star presented lower sensitivity and spatial specificity to detect WM, task-related activations, but also showed equivalent results in the identification of RSNs. Looping Star is expected to particularly benefit auditory and language task fMRI, as well as resting state, sleep, and pediatric studies.

## Acknowledgments

We thank Prof. Haase, Prof. Burschka, and Dr. Menzel for fruitful scientific discussions about the project. The authors thank Brice Fernandez for valued assistance and helpful comments related to resting state analysis.

## References

1. Quirk M, Letendre A, Ciottone R, Lingley J. Anxiety in patients undergoing MR imaging. Radiology 1989;170:463-466.
2. Bandettini PA, Jesmanowicz A, Van Kylen J, Birn RM, Hyde JS. Functional MRI of brain activation induced by scanner acoustic noise. Magn Reson Med 1998;39:410-416.
3. Cho ZH, Chung SC, Lim DW, Wong EK. Effects of the acoustic noise of the gradient systems on fMRI: A study on auditory, motor, and visual cortices. Magn Reson Med 1998;39:331-336.
4. Yakunina N, Kang EK, Kim TS, Min J-H, Kim SS, Nam E-C. Effects of scanner acoustic noise on intrinsic brain activity during auditory stimulation. Neuroradiology 2015;57:1063-1073.
5. Ogawa S, Lee TM, Kay AR. Brain magnetic resonance imaging with contrast dependent on blood oxygenation. Proc Natl Acad Sci U S A 1990;87:9868-9872.
6. Moelker A, Pattynama PMT. Acoustic noise concerns in functional magnetic resonance imaging. Hum Brain Mapp 2003;20:123-141.
7. Mansfield P, Glover PM, Beaumont J. Sound generation in gradient coil structures for MRI. Magn Reson Med 1998;39:539-550.
8. Foster JR, Hall DA, Summerfield AQ, Palmer AR, Bowtell RW. Sound-level measurements and calculations of safe noise dosage during EPI at 3 T. J Magn Reson Imaging 2000;12:157-163.
9. Amaro E, Williams SCR, Shergill SS, et al. Acoustic noise and functional magnetic resonance imaging: Current strategies and future prospects. J Magn Reson Imaging 2002;16:497-510.
10. Tomasi D, Caparelli EC, Chang L, Ernst T. fMRI-acoustic noise alters brain activation during working memory tasks. Neuroimage 2005;27:377-386.
11. Jacob SN, Shear PK, Norris M, et al. Impact of fMRI scanner noise on affective state and attentional performance. J Clin Exp Neurpsychol 2015;37:563-570.
12. Rondinoni C, Amaro E, Cendes F, dos Santos AC, Salmon CEG. Effect of scanner acoustic background noise on strict resting-state fMRI. Braz J Med Biol Res 2013;46:359-367.
13. Andoh J, Ferreira M, Leppert IR, Matsushita R, Pike B, Zatorre RJ. How restful is it with all that noise? Comparison of interleaved silent steady state (ISSS) and conventional imaging in resting-state fMRI. Neuroimage 2017;147:726-735.
14. Bowtell R, Mansfield P. Gradient coil design using active magnetic screening. Magn Reson Med 1991;17:15-21.
15. Edelstein WA, Kidane TK, Taracila V, et al. Active-passive gradient shielding for MRI acoustic noise reduction. Magn Reson Med 2005;53:1013-1037.
16. Li M, Rudd B, Lim TC, Lee J-H. In situ active control of noise in a 4 T MRI scanner. J Magn Reson Imaging 2011;34:662-669.
17. Segbers M, Rizzo Sierra CV, Duifhuis H, Hoogduin JM. Shaping and timing gradient pulses to reduce MRI acoustic noise. Magn Reson Med 2010;64:546-553.
18. Zapp J, Schmitter S, Schad LR. Sinusoidal echo-planar imaging with parallel acquisition technique for reduced acoustic noise in auditory fMRI. J Magn Reson Imaging 2012;36:581-588.
19. Madio DP, Lowe IJ. Ultra-fast imaging using low flip angles and FIDs. Magn Reson Med 1995;34:525-529.
20. Idiyatullin D, Corum C, Park J-Y, Garwood M. Fast and quiet MRI using a swept radiofrequency. J Magn Reson 2006;181:342-349.
21. Weiger M, Pruessmann KP, Hennel F. MRI with zero echo time: Hard versus sweep pulse excitation. Magn Reson Med 2011;66:379-389.
22. Grodzki DM, Jakob PM, Heismann B. Ultrashort echo time imaging using pointwise encoding time reduction with radial acquisition (PETRA). Magn Reson Med 2012;67:510-518.

23. Solana AB, Menini A, Sacolick L, Hehn N, Wiesinger F. Quiet and distortion-free, whole brain BOLD fMRI using T2-prepared RUFIS. Magn Reson Med 2016;75:1402-1412. https://doi.org/10.1002/mrm.25658

24. Wiesinger F, Menini A, Solana AB. Looping Star. Magn Reson Med 2019;81:57-68.

25. Bandettini PA, Wong EC, Hinks RS, Tikofsky RS, Hyde JS. Time course EPI of human brain function during task activation. Magn Reson Med 2005;25:390-397.

26. Friedman L, Glover GH. Report on a multicenter fMRI quality assurance protocol. J Magn Reson Imaging 2006;23:827-839.

27. Owen AM, McMillan KM, Laird AR, Bullmore E. N-back working memory paradigm: A meta-analysis of normative functional neuroimaging studies. Hum Brain Mapp 2005;25:46-59.

28. Behzadi Y, Restom K, Liau J, Liu TT. A component based noise correction method (CompCor) for BOLD and perfusion based fMRI. Neuroimage 2007;37:90-101.

29. Tomasi D, Volkow ND. Functional connectivity hubs in the human brain. Neuroimage 2011;57:908-917.

30. Tzourio-Mazoyer N, Landeau B, Papathanassiou D, et al. Automated anatomical labeling of activations in SPM using a macroscopic anatomical Parcellation of the MNI MRI single-subject brain. Neuroimage 2002; 15:273-289.

31. Kirilina E, Lutti A, Poser BA, Blankenburg F, Weiskopf N. The quest for the best: The impact of different EPI sequences on the sensitivity of random effect fMRI group analyses. Neuroimage 2016;126:49-59.

32. Yarkoni T, Poldrack RA, Nichols TE, Van Essen DC, Wager TD. Large-scale automated synthesis of human functional neuroimaging data. Nat Methods 2011;8:665-670.

33. Constable RT, Skudlarski P, Gore JC. An ROC approach for evaluating functional brain MR imaging and postprocessing protocols. Magn Reson Med 2005;34:57-64.

34. Ljungberg E, Wood T, Solana AB, Kolind S, Williams SC, Wiesinger F, Barker GJ. Silent T1 mapping using the variable flip angle method with B1 correction. Magn Reson Med 2020.

35. Glover GH, Lai S. Self-navigated spiral fMRI: Interleaved versus single-shot. Magn Reson Med 1998;39:361-368.

36. Lin W, Huang F, Simonotto E, Duensing GR, Reykowski A. Off-resonance artifacts correction with convolution in *k*-space (ORACLE). Magn Reson Med 2012;67:1547-1555.

37. Kundu P, Voon V, Balchandani P, Lombardo MV, Poser BA, Bandettini PA. Multiecho fMRI: A review of applications in fMRI denoising and analysis of BOLD signals. Neuroimage 2017;154:59-80.

38. Chiew M, Smith SM, Koopmans PJ, Graedel NN, Blumensath T, Miller KL. K-t FASTER: Acceleration of functional MRI data acquisition using low rank constraints. Magn Reson Med 2014;74:353-364.

39. Thaerig S, Behne N, Schadow J, et al. Sound level dependence of auditory evoked potentials: Simultaneous EEG recording and low-noise fMRI. Int J Psychophysiol 2008;67:235-241.

40. Damestani N, Lythgoe D, Wiesinger F, Solana A, Williams S, Zelaya F. Looping Star silent fMRI: a platform for improving studies of auditory processing. 27th ISMRM Annual Meeting, Montréal, QC, Canada, 11-16 May 2019.